

Dynamics of Nanosatellite Deorbit by Bare Electrodynamic Tether in Low Earth Orbit

R. Zhong* and Z. H. Zhu†

York University, Toronto, Ontario M3J 1P3, Canada

DOI: 10.2514/1.A32336

This paper studies the dynamics of nanosatellite deorbit by a bare electrodynamic tether. The orbital dynamics of the tethered nanosatellite is modeled in Gaussian perturbation equations and the motion-induced voltage-current relationship along the electrodynamic tether is analyzed by using the 2000 International Geomagnetic Reference Field model including up to seventh-order terms and the International Reference Ionosphere 2007 model. The analysis reveals that the high-order magnetic model of Earth affects the dynamic characteristics of the tethered nanosatellite, especially in orbits with high inclination angles, by changing its orbit from circular to elliptical forms. This is beneficial for deorbiting the nanosatellite in near-polar orbits where the electrodynamic force is not as effective as in the equatorial orbit because the denser atmosphere at a lower perigee will provide a larger atmospheric drag. Moreover, the analysis shows that the electrodynamic force is always against the satellite motion in low Earth orbit even when the induced voltage/current across the tether reverses their polarities in near-polar orbits. Compared to the deorbit rate by the atmospheric drag only, the deorbit rate by an electrodynamic tether will be increased by several orders in magnitudes in both equatorial and polar orbits.

Nomenclature

A	= cross-section area of electrodynamic tether, m^2
a	= semimajor axis of orbit, m
A_d	= projected area of nanosatellites for atmospheric drag, m^2
\vec{B}	= magnetic field strength vector, T
B_r, B_θ, B_ϕ	= components of magnetic-field strength vector in spherical coordinates (r, θ, ϕ) , T
C_d	= atmospheric-drag coefficient
d	= diameter of electrodynamic tether, m
e	= eccentricity of orbit
E_m	= projection of motional electric field along electrodynamic tether, $\text{V} \cdot \text{m}^{-1}$
f	= true anomaly of orbit, rad
g_n^m, h_n^m	= Gaussian coefficients of Earth's magnetic model, T
I	= induced current in electrodynamic tether, A
i	= orbital inclination angle, rad
I_0	= unit current, A
\vec{l}	= unit-length vector along electrodynamic tether, from anode end to cathode end
L	= length of electrodynamic tether, m
L_0	= unit length, m
M	= mean anomaly of orbit, rad
m_e, m_i	= mass of electron and ion, kg
n	= mean orbital angular rate, $\text{rad} \cdot \text{s}^{-1}$
n_∞	= unperturbed plasma density, m^{-3}
p	= semilatus rectum of orbit, m
$P_n^m(\theta)$	= Schmidt quasi-normalized associate Legendre functions of degree n and order m
q_e	= electron charge, C
r	= geocentric radius of tethered nanosatellite system, m

Received 12 February 2012; revision received 8 July 2012; accepted for publication 27 July 2012; published online 20 March 2013. Copyright © 2012 by R. Zhong and Z. H. Zhu. Published by the American Institute of Aeronautics and Astronautics, Inc., with permission. Copies of this paper may be made for personal or internal use, on condition that the copier pay the \$10.00 per-copy fee to the Copyright Clearance Center, Inc., 222 Rosewood Drive, Danvers, MA 01923; include the code 1533-6794/13 and \$10.00 in correspondence with the CCC.

*Postdoctoral Fellow, Department of Earth and Space Science and Engineering, 4700 Keele Street.

†Associate Professor, Department of Earth and Space Science and Engineering, 4700 Keele Street; gzhu@yorku.ca. Senior Member AIAA (Corresponding Author).

\vec{r}	= geocentric position vector of tethered nanosatellite system, m
r_0	= reference radius of Earth, m
s	= local coordinate along electrodynamic tether
T, S, W	= perturbative-acceleration components in orbital coordinate system, $\text{m} \cdot \text{s}^{-2}$
$\frac{u}{v}$	= sum of argument of perigee and true anomaly, rad
\vec{v}_r	= orbital-velocity vector of tethered nanosatellite system, $\text{m} \cdot \text{s}^{-1}$
V_p	= relative-velocity vector of tethered nanosatellite system with respect to Earth, $\text{m} \cdot \text{s}^{-1}$
V_t	= motion-induced voltage, V
V_0	= tether voltage, V
γ_C	= unit voltage, V
ϵ_B	= dimensionless current at cathode end
θ	= dimensionless length of positively biased segment of electrodynamic tether
λ_A	= colatitude, defined as $\theta = \pi/2 - \text{latitude}$, rad
ρ	= dimensionless voltage at anode end
σ	= atmospheric density, $\text{kg} \cdot \text{m}^{-3}$
ϕ	= electric conductivity of electrodynamic tether, $\Omega \cdot \text{m}^{-1}$
Ω	= longitude, rad
ω	= longitude of ascending node of orbit, rad
ω_E	= argument of perigee of orbit, rad
	= rotational-velocity vector of Earth, $\text{rad} \cdot \text{s}^{-1}$

I. Introduction

SPACE tether technology has great potential in enabling a broad range of scientific and engineering tasks, such as long-baseline interferometer [1], power generation [2], satellite formation flying [3], space transportation [4], and orbital maneuver [5,6]. Over the past five decades 26 orbital and suborbital missions have flown or planned to fly with tether lengths ranging from 10 m to 30 km (Table 1). Among them 12 missions flew or planned to fly with electrodynamic tethers (EDT) to test the propellantless propulsion technology through electromagnetic interaction of EDT with Earth's magnetic field [7]. One of the most appealing applications of this EDT technology is in space-debris prevention and mitigation [8]. Currently, over 19,000 satellites and other traceable objects (larger than 5 cm) are in orbits around the Earth. The estimated population of particles between 1 and 5 cm in diameter is approximately 500,000 according to the latest NASA estimation. More specifically, a study shows [9] that the cumulative distribution of the collision-generated

Table 1 Summary of space tether missions

Name	Date	Agency	Orbit	Length	EDT	Description
Gemini 11	1967	NASA	LEO	30 m	No	Stable by spinning at 0.15 rpm
Gemini 12	1967	NASA	LEO	30 m	No	Stable swing about local vertical
H-9M-69	1980	NASA	Suborbital	500 m	Yes	Partially deployed
S-520-2	1981	NASA/ISAS ^a	Suborbital	500 m	Yes	Partially deployed
Charge-1	1983	NASA/ISAS ^a	Suborbital	500 m	Yes	Fully deployed
Charge-2	1984	NASA/ISAS ^a	Suborbital	500 m	Yes	Fully deployed
Oedipus-A	1989	CSA/NASA	Suborbital	958 m	No	Stable by spinning at 0.7 rpm with spin axis aligned with magnetic field
Charge-2B	1992	NASA	Suborbital	500 m	Yes	Fully deployed
TSS-1	1992	NASA/ISA ^c	LEO	260 m	Yes	Partially deployed and retrieved
SEDS-1	1993	NASA	LEO	20 km	No	Fully downward deployed, swing, and cut
PMG	1993	NASA	LEO	500 m	Yes	Upward deployed
SED-2	1994	NASA	LEO	20 km	No	Fully deployed in local vertical
Oedipus-C	1995	CSA/NASA	Suborbital	1170 m	No	Stable by spinning at 0.7 rpm with spin axis aligned with magnetic field
TSS-1R	1996	NASA/ISA ^c	LEO	19.6 km	Yes	Almost fully deployed but severed by arcing
TiPS	1996	NRO ^d /NRL ^e	LEO	4 km	No	Survived 12 yrs on-orbit
YES	1997	TUD ^f	GTO	35 km	No	Not deployed to avoid a collision with other spacecraft
ATEx	1999	NRL ^e	LEO	6 km	No	Partially deployed
PICOSAT1.0	2000	Aerospace Corp.	LEO	30 m	No	Operated for 3 days
PICOSAT1.1	2000	Aerospace Corp.	LEO	30 m	No	Tested storage effects on the system
ProSEDS	2003	NASA	LEO	15 km	Yes	Hardware built, mission cancelled
DTUsat-1	2003	TUD ^f	LEO	450 m	Yes	Nanosatellite failed in space
MAST	2007	NASA	LEO	1 km	No	Tether failed to deploy
YES-2	2007	ESA	LEO	30 km	No	Fully deployed and cut off
Cute-1.7 +APDII	2008	TIT ^g	LEO	10 m	Yes	Tether failed to deploy
STARS	2009	Kagawa Univ.	LEO	10 m	No	Space tethered robot mission, tether deployed
T-Rex	2010	JAXA ^h	Suborbital	300 m	Yes	Fully deployed but current not measured

debris potential in low Earth orbit (LEO) peaks around orbital inclination angles at 71–74°, 81–83°, and sun-synchronized orbit, whereas the distribution of operational satellites in LEO concentrates around orbital-inclination angles at 45–55°, 80–90°, and sun-synchronized orbit. These objects will inevitably lead to spacecraft and/or debris collision in space, which is evidenced by the first-ever satellite collision between Iridium 33 and Cosmos 2251 in 2009 [10]. Because the LEO is not an unlimited resource that can accommodate the ever-increasing quantity of space debris, it is imperative to develop space-debris mitigation and removal measures such as the self-deorbit of spacecraft at the end of mission and spent upper stages of rockets.

Recently there is renewed interest in the EDT-propulsion technology in NASA [11], Japan Aerospace Exploration Agency (JAXA) [12], and other leading space agencies [13] due to its potential application in space-debris mitigation and removal. Compared to other deorbit concepts or technologies commonly used by larger spacecraft such as the rocket or thruster, EDT-propulsion technology has the advantages of low mass, compact size, propellantless, and no requirement for spacecraft to be operational during the deorbiting process [14]. These merits of EDT-propulsion technology make it most appealing for the fast growing micro/nanosatellites because their small mass/size ratio limits the use of the techniques commonly employed by larger spacecraft.

The concept of using EDT's electrodynamic propulsion to remove unusable spacecraft was suggested initially by Grossi [15] and then developed by other researchers [16,17]. More specifically, using a bare tether as anode to collect electrons appears particularly suitable for the deorbit purpose because of its simplicity, reliability, and high electron-collection efficiency [18–22]. Although EDT-propulsion technology has been extensively studied and many EDT missions have flown in the past, some key technologies still remain untested on the drawing board [23], such as the bare-tether current generation and the deorbit efficiency of EDT-propulsion technology in near-polar orbits or orbits with high inclination angles. It is widely believed that deorbiting spacecraft by EDT in near-polar orbits is inefficient because the motional electric field of EDT will be minimized in these orbits [24]. In addition, there is little detailed study on deorbiting nanosatellites using EDT-propulsion technology where the EDT length ranges from a few meters to a few hundred meters. This has

motivated the current study of deorbiting nanosatellites using a bare and short EDT. In the following study we focus our attentions on: 1) the feasibility of a short EDT for deorbiting nanosatellites, 2) the impact of irregular variation of Earth's magnetic field on EDT propulsion by considering the higher order corrections of the 2000 International Geomagnetic Reference Field (IGRF) model to the commonly used dipole-magnetic-field model, and 3) the EDT deorbit efficiency in polar orbits.

This paper contains five sections. Following this brief introductory section, Sec. II provides a detailed account of the dynamics of the EDT-nanosatellite system. In Sec. III we discuss the boundary conditions for the dynamic systems of the EDT-nanosatellite system and solution procedures. In Sec. IV we conduct detailed deorbit-dynamic simulations of the EDT-nanosatellite system. Finally, we conclude the paper in Sec. V.

II. Dynamics of Eletrodynamic-Tether-Nanosatellite System

A. Orbital Dynamic Equations of Tethered-Nanosatellite System

Consider two nanosatellites connected by a bare and short EDT in LEO. For simplicity it is assumed that the EDT is 1) rigid due to its short length and 2) stabilized in the local vertical by gravity gradient with tether libration motion neglected. Based on these assumptions one can reasonably simplify the tethered nanosatellite system as a point mass in the orbit-dynamic analysis because the size of the system (nanosatellites with a tether shorter than 1 km) is extremely small compared to the radius of Earth. Thus, the motion of the EDT-nanosatellite system can be considered in a geocentric inertial frame of Earth ($Oxyz$) with the origin at Earth's center, the x -axis directing to the point of vernal equinox, the z -axis aligning with the rotation axis of Earth, and the y -axis completing the system with a right-hand coordinate system (see Fig. 1). Accordingly, the orbital-dynamic equations of the system can be described in the form of Gaussian perturbation equations [25] in Eq. (1), such as

$$\frac{da}{dt} = \frac{2}{n\sqrt{1-e^2}} \left(Te \sin f + S \frac{p}{r} \right) \quad (1a)$$

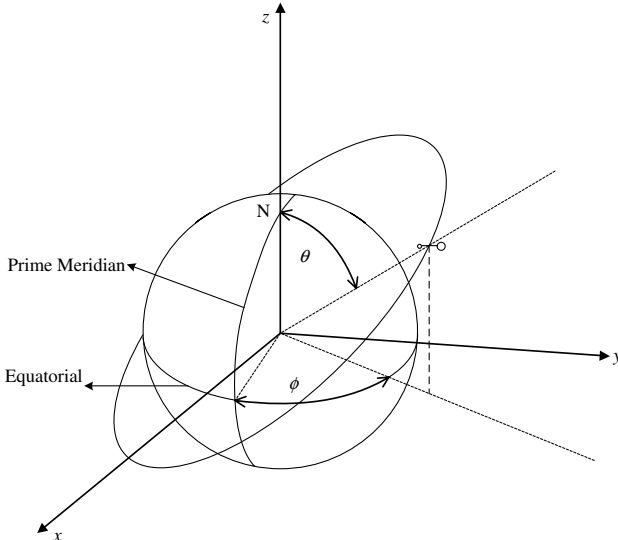


Fig. 1 Illustration of system coordinates.

$$\frac{d\Omega}{dt} = \frac{Wr \sin u}{na^2 \sqrt{1-e^2} \sin i} \quad (1b)$$

$$\frac{di}{dt} = \frac{Wr \cos u}{na^2 \sqrt{1-e^2}} \quad (1c)$$

$$\begin{aligned} \frac{de_x}{dt} &= \frac{\sqrt{1-e^2}}{na} \left\{ T \sin u + S \left[\left(1 + \frac{r}{p} \right) \cos u + \frac{r}{p} e_x \right] \right\} \\ &+ \frac{d\Omega}{dt} e_y \cos i \end{aligned} \quad (1d)$$

$$\begin{aligned} \frac{de_y}{dt} &= \frac{\sqrt{1-e^2}}{na} \left\{ -T \cos u + S \left[\left(1 + \frac{r}{p} \right) \sin u + \frac{r}{p} e_y \right] \right\} \\ &- \frac{d\Omega}{dt} e_x \cos i \end{aligned} \quad (1e)$$

$$\begin{aligned} \frac{d\eta}{dt} &= n - \frac{1}{na} \left[T \left(\frac{2r}{a} + \frac{\sqrt{1-e^2}}{1+\sqrt{1-e^2}} e \cos f \right) \right. \\ &\left. - S \left(1 + \frac{r}{p} \right) \frac{\sqrt{1-e^2}}{1+\sqrt{1-e^2}} e \sin f \right] - \frac{Wr \cos i \sin u}{na^2 \sqrt{1-e^2} \sin i} \end{aligned} \quad (1f)$$

Here $e_x (=e \cos \omega)$, $e_y (=e \sin \omega)$, and $\eta (=M + \omega)$ are used to replace the classical orbital elements e , M , and ω to avoid the singularity when the eccentricity of orbit is small. The perturbative-acceleration components T and S are in the orbital plane with T being the radial component and S perpendicular to T and pointing to the direction of tethered-nanosatellite motion. The third perturbative-acceleration component W completes a right-hand system.

The perturbative accelerations (T , S , W) in Eq. (1) are caused by orbital perturbation forces, namely 1) Earth's atmospheric drag, 2) the nonhomogeneity and oblateness of Earth, 3) the electrodynamic force acting on the current-carrying EDT, 4) the lunisolar gravitational perturbation forces, 5) the solar radiation pressure, and 6) the spacecraft thrust. In the current study we will consider only the first three perturbation forces in the deorbit-dynamic analysis because the effects of lunisolar-gravitational perturbation and the solar-radiation pressure are small and negligible compared to the first three perturbation forces in LEO. In addition, the EDT-nanosatellite system is assumed thrustless during the deorbit process. For the sake

of simplicity in analysis we further assume that the atmosphere rotates with the Earth in the same rate.

B. Atmospheric Drag Force

The EDT-nanosatellite system in LEO will experience atmospheric drag force due to the momentum exchange between the free molecules and the arresting surfaces of EDT and nanosatellites. Earth's atmospheric drag force acting on the nanosatellites $\mathbf{F}_{A,s}$ and the element length ds of EDT $d\mathbf{F}_{A,t}$ are calculated using the well-known square law such that

$$\mathbf{F}_{A,s} = -\frac{1}{2} \rho C_d |\vec{v}_r| \vec{v}_r A_d \quad (2a)$$

$$d\mathbf{F}_{A,t} = -\frac{1}{2} \rho C_d d |\vec{v}_r| \vec{v}_r ds \quad (2b)$$

The relative velocity of the EDT-nanosatellite system with respect to Earth can be determined as

$$\vec{v}_r = \vec{v} - \vec{\omega}_E \times \vec{r} \quad (3)$$

For the EDT with circular cross section its drag coefficient C_d can be simplified as a constant equal to 2.2 [26] by considering a circular cylinder moving in a free-molecular hyperthermal flow in space. From the same literature the drag coefficient of a cubic-shape nanosatellite is a constant of 1.6. However, the density of Earth's atmosphere varies rapidly over the altitude. In this work the 1976 atmospheric model of U. S. Standard Atmosphere[‡] is adopted to calculate the atmospheric density at any given altitude between sea level and 1,000 km. This model matches quite well with the simple empirical model by Carroll [27] when the orbital altitude is between 200 km and 800 km. However, it is more accurate for orbital altitudes above 800 km for orbit-lifetime calculation where the Carroll's model is too conservative [28].

C. Perturbation Force Due to Earth's Oblateness

The oblateness of Earth attracts satellites orbiting around Earth towards its equator by imposing a torque on the satellites in any orbital plane that cross the equator at an angle causing the direction of the orbital-angular-momentum vector to regress. The daily increase of the ascending node caused by J_2 perturbation, which is the major term of the oblateness perturbation, can be described as [25]

$$\Delta\Omega = -9.97 \left(\frac{r_0}{a} \right)^{7/2} \cos i \quad (4)$$

The reference radius of Earth r_0 is 6371.2 km. In this paper, we will examine the impact of this effect on the deorbit rate of a tethered nanosatellite system.

D. ElectrodynamiC Force

As a bare conductive EDT crosses Earth's magnetic field at the orbital velocity a motional electric field will be induced, and its projection along the EDT length E_m can be expressed as [28]

$$E_m = \frac{dV_p}{ds} = (\vec{v}_r \times \vec{B}) \cdot \vec{l} \quad (5)$$

Because the Earth's magnetic field varies irregularly in the geocentric body-fixed frame of Earth, a higher-order and inclined Earth's magnetic model, the IGRF2000 model [29,30], is adopted in the current study, and its magnetic-field strength can be described in the body-fixed frame of Earth such that

[‡]The U.S Standard Atmosphere, U.S. Government Printing Office, 1976.

$$\mathbf{B} = \begin{cases} \begin{aligned} & B_r \\ & B_\theta \\ & B_\phi \end{aligned} \end{cases}$$

$$= \begin{cases} \sum_{n=1}^{\infty} \left(\frac{r_0}{r}\right)^{n+2} (n+1) \sum_{m=0}^n [g_n^m \cos(m\phi) + h_n^m \sin(m\phi)] P_n^m(\theta) \\ - \sum_{n=1}^{\infty} \left(\frac{r_0}{r}\right)^{n+2} \sum_{m=0}^n [g_n^m \cos(m\phi) + h_n^m \sin(m\phi)] \frac{\partial P_n^m(\theta)}{\partial \theta} \\ \frac{-1}{\sin \theta} \sum_{n=1}^{\infty} \left(\frac{r_0}{r}\right)^{n+2} \sum_{m=0}^n m [-g_n^m \sin(m\phi) + h_n^m \cos(m\phi)] P_n^m(\theta) \end{cases}$$

(6)

Detailed expressions of the coefficients in Eq. (6) can be found in the literature [29].

It should be noted that the most commonly used model of Earth's magnetic field in literature is the inclined-dipole model [31]. The angle between the dipole axis and Earth's self-rotation axis is about 11.5 deg, and the dipole moment is $7.788 \times 10^{22} \text{ A} \cdot \text{m}^2$. The inclined-dipole model is actually the first-order approximation of the IGRF2000 model expressed in Eq. (6), and some works [32] used this first-order approximation of IGRF2000 model. However, the correction due to the higher-order terms in Eq. (6) becomes not negligible for the EDT orbiting with high inclination angles. For instance, if the EDT is moving in a circular polar orbit, the motional electric field along the tether can be deduced from Eq. (5) approximately, such as

$$E_m = B_\phi \sqrt{\mu/r} - B_\theta \omega_E r \sin \theta \quad (7)$$

Earth's rotational speed ω_E is about $7.3 \times 10^{-5} \text{ rad} \cdot \text{s}^{-1}$, and the maximum corotational speed $\omega_E r \sin \theta$ is less than one-tenth of the orbital speed $\sqrt{\mu/r}$ if the orbital height is equal to 1000 km. Thus, Eq. (7) indicates that the component B_ϕ is the major contributor of magnetic field to the motional electric field in a circular polar orbit. If one adopts the inclined-dipole model or the first-order approximation of the IGRF2000 model, the component B_ϕ at any point is independent of the latitude, such as

$$B_\phi = \left(\frac{r_0}{r}\right)^3 [g_1^1 \sin(\phi) - h_1^1 \cos(\phi)] \quad (8)$$

Meanwhile, numerical calculation of Eq. (6) indicates that the average value of B_ϕ near the south pole is approximately eight times greater than the north pole. Thus, the oversimplification of the dipole model leads to an unfavorable estimation of deorbit rate of EDT-nanosatellite system in the polar and near-polar orbits.

To understand more accurately the irregularity effect of Earth's magnetic field on the induced motional electric field, which is critical in the EDT-dynamic analysis, we calculate and compare the variations of motional electric field E_m by Eq. (7) for a circular orbit at an altitude of 1,000 km by different orders of approximation. Figure 2 shows the variation of E_m using the first-order approximation, where

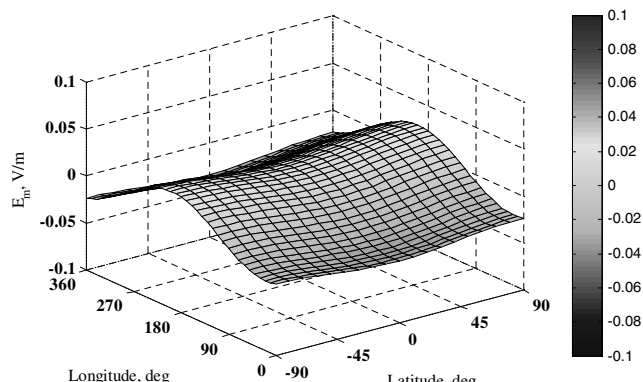


Fig. 2 E_m variation of the first-order approximation with respect to longitude and latitude.

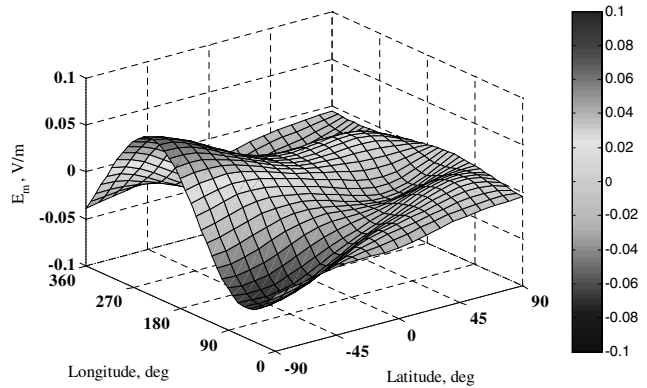


Fig. 3 E_m variation of the seventh-order approximation with respect to longitude and latitude.

the E_m does not change much for a given longitude as indicated by Eq. (7). This implies the electrodynamic force exerted on the EDT will be almost the same as the nanosatellite orbiting from the south pole to the north pole if the orbital plane remains stationary with respect to Earth. Figures 3 and 4 show the variations of E_m that includes 1st to 7th and 1st to 13th order terms of Earth's magnetic field, respectively. They indicate clearly that the E_m varies not only in the longitude but also the latitude directions. The induced motional electric field is greater at the south pole than the north pole. This will cause a secular growth of the eccentricity of EDT's orbit and consequently the perigee of the polar orbit moving closer to the north pole gradually. As a result, the EDT-nanosatellite system will experience larger atmospheric drag at the perigee due to the higher atmospheric density, which in turn accelerates the deorbit rate of the EDT-nanosatellite system. Finally, the E_m calculated using the seventh-order approximation of the magnetic field in Fig. 3 is almost the same as the 13th-order approximation in Fig. 4 with the mean error less than 1%. Therefore, the seventh-order model of Earth's magnetic field is adopted in the following sections for the compromise between computational accuracy and efficiency.

Furthermore, the resulting motional electric field will make the EDT partially positive and partially negative charged relative to the ambient ionospheric plasma, depending on the difference between the motion-induced voltage V_p and the tether voltage V_t that obeys Ohm's law (see Fig. 5). Consequently, the electrons in the ionosphere will be collected by the positively biased part of EDT, whereas the ions will be collected by the negatively biased part of EDT if the EDT is bare and its length is several orders of magnitude larger than its diameter [33]. If there is a device at the end of the EDT to expel the electrons back into the ionosphere to complete the current loop, as shown in Fig. 5, a current will be generated in the EDT. Assuming the space-charge or magnetic-guiding effects are negligible, the induced current is orbital-motion limited and can be described as [32,33]

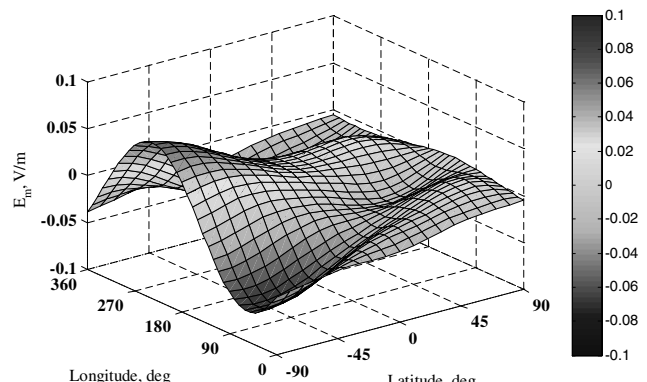


Fig. 4 E_m variation of the 13th-order approximation with respect to longitude and latitude.

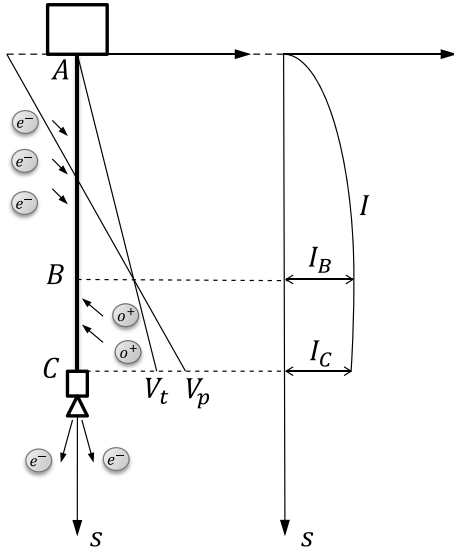


Fig. 5 Scheme of a bare electrodynamic tether and voltage-current variation. Points A and C denote the anodic and cathodic ends, respectively, and B is the point with zero potential bias.

$$\frac{dI}{ds} = q_e n_\infty d \begin{cases} (2q_e \Delta V / m_e)^{1/2} & \text{if } V_t > V_p \\ -(2q_e \Delta V / m_i)^{1/2} & \text{if } V_t < V_p \end{cases} \quad (9)$$

The relative voltage of the EDT with respect to the ambient ionospheric plasma varies due to the ohmic loss depending on the induced current flow I . Therefore, the relationship among the relative voltage, the induced current, and the motional electric field can be written as

$$\frac{d\Delta V}{ds} = \frac{I}{\sigma A} - E_m \quad (10)$$

Generally, the numbers of ions collected are much fewer than electrons and can be neglected because the mass of an ion is much greater than that of an electron. Therefore, we can assume that the induced current is constant ($dI/ds \approx 0$) in the negatively biased segment \overline{BC} of the EDT. The induced current in the EDT will interact with the magnetic field of Earth to generate the Lorentz or electrodynamic force such that

$$d\mathbf{F}_B = -\vec{\mathbf{B}} \times \vec{I} ds \quad (11)$$

Correspondingly, the power dissipated by the EDT is

$$\begin{aligned} P &= \int_0^L \vec{v}_r \cdot d\mathbf{F}_B = - \int_0^L \vec{v}_r \cdot (\vec{\mathbf{B}} \times \vec{I}) I ds \\ &= - \int_0^L (\vec{v}_r \times \vec{\mathbf{B}}) \cdot \vec{I} I ds \end{aligned} \quad (12)$$

Substituting Eq. (5) into Eq. (12) leads to

$$P = - \int_0^L E_m I ds = - \int_0^L I dV_p \quad (13)$$

Because the motional electric field E_m drives the induced current I , the product of $E_m I \geq 0$ and the dissipated power is always negative. Furthermore, Eq. (13) indicates that the mechanical power is equivalent to the heat dissipated by the current in the EDT. For LEO the EDT's relative velocity \vec{v}_r is the same direction as the EDT's orbital velocity \vec{v} . Thus, the projection of the induced Lorentz/electrodynamic force in the orbital plane is always against the orbital motion of EDT even in the case of polar orbit where the induced current in the EDT reverses its direction as the EDT moves from the north pole to the south pole. This is the theoretical foundation of

deorbiting spacecraft by EDT in LEO, which uses the electrodynamic force as a drag to decrease the EDT's orbital altitude.

III. Boundary Conditions and Solution Procedure

To solve the EDT deorbit dynamics in Eq. (1) it is critical to first determine the induced current that is governed by Eqs. (9) and (10). Let us introduce three dimensionless variables per [33] such that

$$\varepsilon = s/L_0, \quad \gamma = I/I_0, \quad \lambda = \Delta V/V_0 \quad (14)$$

The unit length, current, and voltage in Eq. (14) are defined as follows:

$$L_0 = \left(\frac{9\pi m_e \sigma^2 E_m A}{128 q_e^3 n_\infty^2} \right)^{1/3}, \quad I_0 = \sigma E_m A, \quad V_0 = E_m L_0 \quad (15)$$

Note that I_0 is also called the short-circuit current in literature.

Substituting Eqs. (14) and (15) into Eqs. (9) and (10) leads to the dimensionless voltage-current relationships such that

$$\frac{d\gamma}{d\varepsilon} = \frac{3}{4} \sqrt{\lambda} \quad (16)$$

$$\frac{d\lambda}{d\varepsilon} = \gamma - 1 \quad (17)$$

with boundary conditions:

$$\varepsilon = 0: \gamma = 0, \lambda = \lambda_A \quad \text{and} \quad \varepsilon = \varepsilon_B: \gamma = \gamma_B = \gamma_C, \lambda = 0$$

Integrating Eqs. (16) and (17) with the given boundary conditions results in the following expressions

$$\lambda_A = (2\gamma_C - \gamma_C^2)^{2/3} \quad (18)$$

$$\varepsilon_B = \int_0^{\lambda_A} (\lambda^{3/2} - \lambda_A^{3/2} + 1)^{-1/2} d\lambda \quad (19)$$

Equations (18) and (19) contain three unknowns: the voltage bias at the anode end, λ_A (the beginning point of EDT); the current at the cathode or the maximum current generated by an EDT, γ_C ; and the length of positively biased segment of EDT AB , ε_B , respectively. Therefore, additional boundary conditions are required to determine these unknowns. These boundary conditions are usually determined by mission objectives and the electron-emitting devices at the end of EDT. Two commonly used boundary conditions are:

1) The current at the cathode end γ_C is known. If the electron-emitting device is determined, the current at the cathode end is a design parameter that can be determined in advance. Thus, the length of positively biased segment of EDT and the potential bias at the anode end can be calculated directly from Eqs. (18) and (19), and then Eqs. (16) and (17) can be integrated. In this case, the EDT is used for electrodynamic drag and power generation, which usually has a voltage drop at the cathode end over the electric load.

2) The EDT is completely positive biased. For the purpose of investigating the maximum possible deorbiting capacity of an EDT we assumed that the EDT is completely positive biased. In this situation the parameter ε_B is a known constant, and the EDT is used for electrodynamic drag only because there is no voltage drop at the cathode due to the electric load and the voltage drop over the electron-emitting device is assumed small and negligible. This boundary condition is used in the EDT-deorbit-dynamic simulations in the next section.

Once the induced current is determined the electrodynamic force acting on the current-carrying EDT can be calculated by Eq. (11). Consequently, the orbital-dynamic equation, Eq. (1), can be easily solved because the other two perturbation forces (the atmospheric

Table 2 Parameters of an EDT-nanosatellite system [23]

Parameters	Values
Mass of primary satellite	5.0 kg
Mass of secondary satellite	1.75 kg
Mass of tether	0.25 kg
Dimensions of primary satellite	$0.2 \times 0.2 \times 0.2$ m
Dimensions of secondary satellite	$0.1 \times 0.17 \times 0.1$ m
Tether length	500 m
Tether diameter	0.0005 m
Tether electric conductivity (aluminum)	$3.4014 \times 10^7 \Omega^{-1} \text{m}^{-1}$
Drag coefficients	2.2 (tether) and 1.6 (end satellites)
Orbit altitudes	250 ~ 1000 km
Orbit inclination	0 ~ 90 deg

drag and the oblateness of the Earth) are simply the functions of the EDT's velocity and orbital parameters.

IV. Results and Discussion

A. System Parameters

Parameters used in this paper are defined from a mission-concept study proposed for engineering and scientific applications using the nanosatellite with an electrodynamic tether [23]. The size of the EDT is determined subject to hardware constraints and mission objectives. Values of major parameters are listed in Table 2. The ionospheric plasma density is calculated by the 2007 International Reference Ionosphere model [34].

B. Deorbit of Tethered Nanosatellite System by Atmospheric Drag Only

To investigate the efficiency of EDT propulsion in deorbiting a nanosatellite system, we first establish a deorbit baseline by considering the atmospheric drag only. It is assumed that the EDT-nanosatellite system initially runs in a circular orbit at an altitude of 1000 km, and the targeted altitude is 250 km. In addition to the atmospheric drag, we also investigated the impacts of Earth's oblateness and orbital inclination angle on the orbit lifetime of an EDT-nanosatellite system together with the atmospheric drag.

Figure 6 shows the estimated orbit lifetime of the EDT-nanosatellite system initially running in a polar orbit with and without Earth's oblateness perturbation (J_2 , J_3 , and J_4 effects are considered). The tethered system is in a polar orbit and subjected to the atmospheric drag only. It is found that the oblateness perturbation does increase the orbit eccentricity slightly, as shown in Fig. 6a, causing the altitude of the system to oscillate at the orbit frequency. As a result, the total orbit lifetime increases by roughly 1% compared to the case without the effect of oblateness perturbation, as shown in

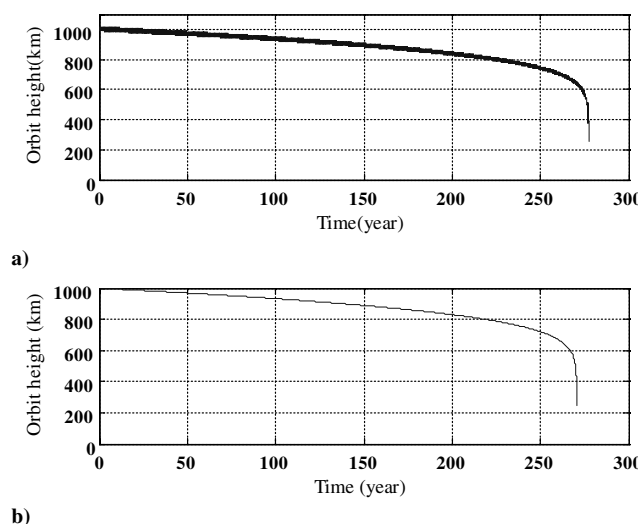


Fig. 6 Deorbit rate of nanosatellite by atmospheric drag only in a polar orbit a) with and b) without Earth's oblateness perturbation.

Table 3 Nanosatellite deorbit time with different orbital inclination (oblateness perturbation not included)

Orbital inclination, deg	Deorbit time, yr
0	328
25	317
50	300
75	281
82	276
90	271

Fig. 6b. This is consistent with the analysis of Wamock and Cochran [35] and is reasonable considering the small length of the EDT (500 m) in consideration. Therefore, the effect of Earth's oblateness is very small and has been neglected in the following EDT-deorbit analysis. In addition, the oblateness perturbation results in a short period effect that reduces significantly the numerical time-integration step size for Eq. (1). The neglect of Earth's oblateness perturbation can increase the computational efficiency and reduce the accumulated errors in the orbit-lifetime analysis.

Next, Table 3 gives a summary of the orbit lifetime of the EDT nanosatellite running in the orbits with different orbital inclination angles. It is shown that the total orbit lifetime increases as the inclination angle of the orbit decreases, up to 21% from the polar to equatorial orbit (here the effect of the inhomogeneous shape of Earth on the true orbital height is not considered). The reason is that the magnitude of relative velocity of the EDT-nanosatellite system with respect to the atmosphere reduces as the inclination angle i decreases from 90 deg as indicated by Eq. (3). This effect is quite significant at high orbital altitudes and diminishes as the orbital altitude reduces below 700 km [28]. Nevertheless, the deorbit time is very long (greater than 200 years) for all inclination angles, which is unacceptable for the space-debris mitigation. The deorbit rate is especially small when the orbit altitude is above 700 km. This necessitates the study for effective deorbit means to reduce the orbit lifetime to less than 25 years as required [14].

C. Electrodynamic-Tether Voltage and Current Induced by Orbital Motion

In this section, we investigated the impacts of orbital inclination angles and altitudes on the induced voltage that is critical for the satellite-deorbit rate. As mentioned in preceding sections, the induced motional electric field E_m depends on the local strength of Earth's magnetic field that varies irregularly in the latitude and longitude directions. Accordingly, we adopted higher-order terms up to seventh order here in evaluating the local strength of Earth's magnetic field to account for its irregular variation. For the sake of simplicity it is assumed that 1) the distributions of magnetic-field

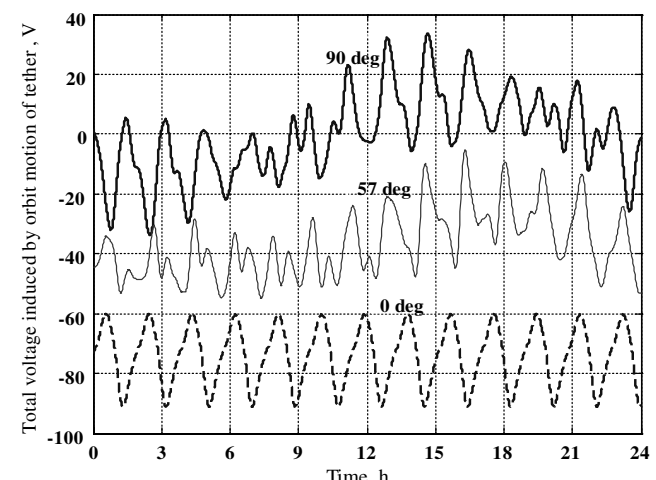


Fig. 7 Induced-voltage variations with respect to orbital inclination angles (orbit altitude: 1000 km).

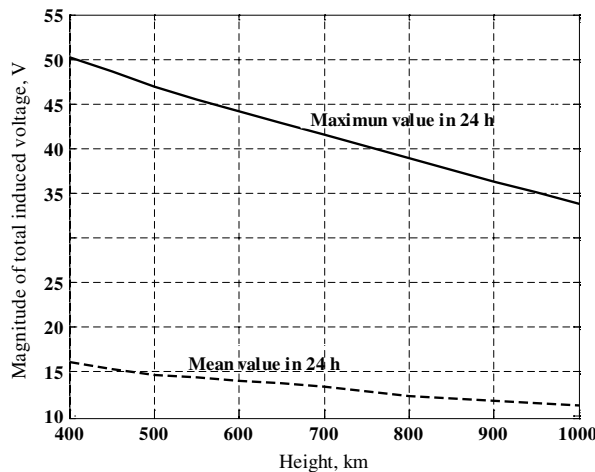


Fig. 8 Induced EDT voltage versus orbital altitude (orbital inclination: 90 deg).

strength and orbital velocity along the EDT are constant because of the EDT's short length (500 m) compared with Earth's radius and 2) the full length of EDT is positively biased.

The analysis results of motion-induced voltage and current and electrodynamic force are shown in Figs. 7–10 where a descending process of an EDT-nanosatellite system was simulated with different orbital inclination angles and altitudes for a period of 24 h. Figure 7 shows that the magnitude of induced voltage increases as the inclination angle decreases. This is reasonable because the directions of relative orbital velocity and local magnetic field are almost collinear in a polar orbit where only the small component along the latitude direction of the magnetic field contributes to the induced voltage. Furthermore, the induced voltage will reverse its direction during the 24-h period when the inclination angle of orbit exceeds certain values due to the inclination of the axis of Earth's magnetic field relative to Earth's rotational axis. Therefore, the EDT system in orbits with higher inclination angles requires electron emitters at both ends of the EDT in order to generate current in the EDT all the time. The change of induced-voltage polarity or current direction disappears as the inclination angle decreases beyond a certain extent where the longitudinal component of Earth's magnetic field becomes the major contributor to the motional electric field. The critical inclination angle is about 57 deg in our case (considering the situation of different orbital altitudes) as shown in Fig. 7. In addition to the inclination angles, Fig. 8 shows the influence of orbital altitudes on the induced voltage, where the maximum and mean values of induced voltage in 24 h are plotted against the orbital altitudes. Clearly, the magnitudes of both the maximum and mean values of induced voltage increase as orbital altitude decreases due to the stronger

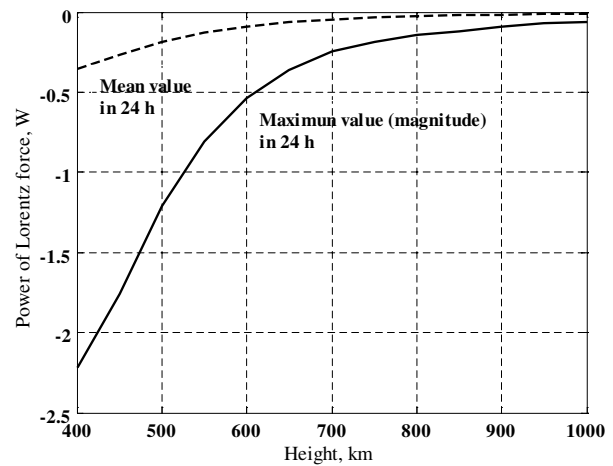


Fig. 10 Power of Lorentz force versus orbital altitude (orbital inclination: 90 deg).

magnetic-field strength at lower altitudes. This in turn increases the magnitude of maximum current in the EDT and the power of Lorentz force during the deorbit process, as shown in Figs. 9 and 10, leading to a higher deorbit rate. Finally, the electron density also increases as the orbital altitude decreases, if the orbital altitude is over 400 km, making the current and the dissipated power increase more quickly than the induced voltage. Details will be given in the next section.

D. Deorbit of Nanosatellite with Electrodynamic Force and Atmospheric Drag

This section presents the analysis results of deorbiting the EDT-nanosatellite system under atmospheric drag and electrodynamic force simultaneously. Figure 11 shows the deorbit rates with different orbital inclination angles. It is found that the total deorbit lifetime is reduced significantly compared with atmospheric drag only shown in Table 3. This becomes more obvious when the system altitude is above 700 km. Deorbit by the EDT works much better for orbits with smaller inclination angles because the induced voltage is much higher as shown in Fig. 7. However, the deorbit time of the EDT with a large inclination angle is also acceptable (less than 25 years). Figures 12 and 13 show the variations of electron density and deorbit forces (the atmospheric drag and the effective electrodynamic force that is defined as its projection in the direction of the plasma relative to the EDT motion) over the orbital altitude in a polar orbit. It can be seen in Fig. 12 that the electron density increases as the orbital altitude decreases and reaches maximum between 300 and 400 km resulting in a larger current in the EDT as indicated in Fig. 9. The scattering electron density at a given orbital altitude represents its variations in the latitude direction. Furthermore, Fig. 13 shows that

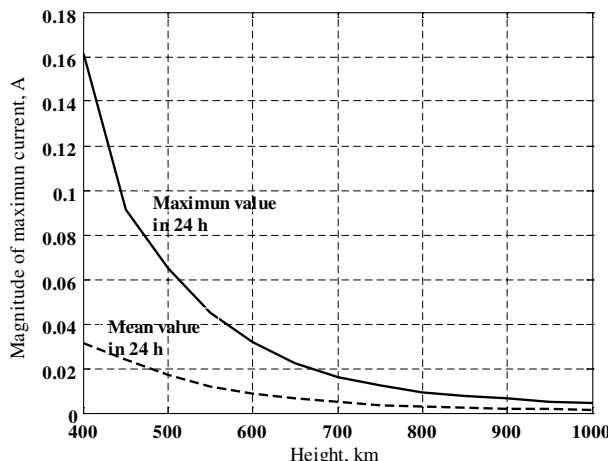


Fig. 9 Current at cathode versus orbital altitude (orbital inclination: 90 deg).

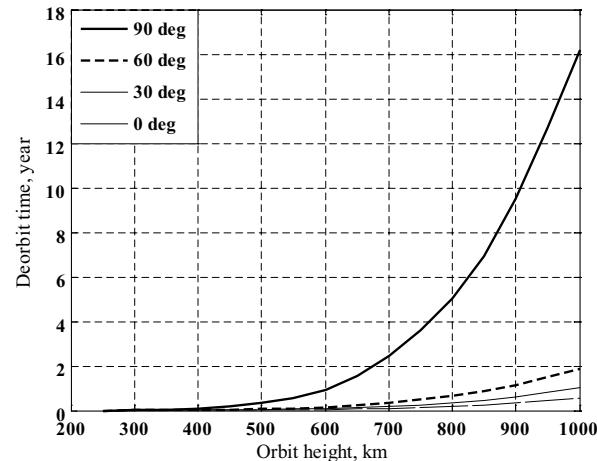


Fig. 11 Deorbit rates of nanosatellites subject to electrodynamic force and atmospheric drag with different orbital inclination angles.

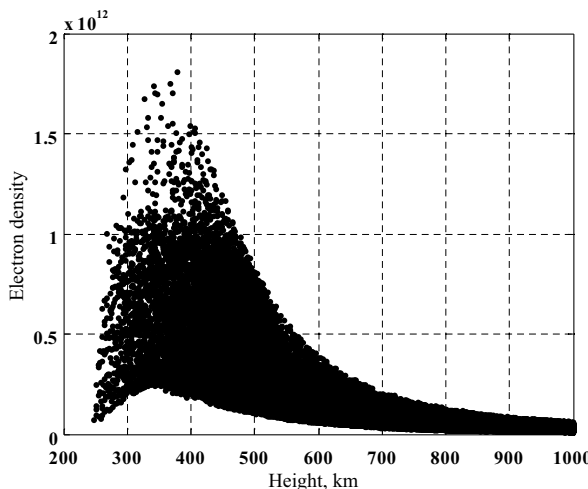


Fig. 12 Variation of electron density of a polar orbit over orbital altitude.

the atmospheric drag is dominating if the orbital altitude is below 400 km, whereas the electrodynamic force is more effective if the orbital altitude is above 700 km. Figure 14 gives the detailed view of two deorbit forces over 700 km, which shows that the electrodynamic force is much greater than the atmospheric drag by one or two orders of magnitude, making EDT a very promising choice for deorbiting nanosatellites from orbits higher than 700 km, even if the orbital inclination is large.

The deorbit time history of a fully positively biased EDT with inclination angles ranging from 0 to 90 deg are shown in Figs. 15 and 16. As expected, Fig. 15 shows that the nanosatellite in an equatorial orbit (zero inclination angle) is deorbited very quickly by the EDT in less than one year compared with 328 years with the atmospheric drag only as shown in Table 3. The situation in the polar orbit (90 deg inclination angle) is more complicated. Although Fig. 16 shows that the EDT reduces the deorbit time from 271 years to about 16 years, the results reveal an interesting phenomenon. The EDT-nanosatellite system starts with a circular polar orbit, and then its orbit gradually changes into an elliptical one due to Earth's irregular magnetic field. The eccentricity of the orbit increases as the orbital altitude decreases due to the cumulative effect of the electrodynamic-drag difference between the south and north poles. The average strength of the local magnetic field's longitudinal component B_ϕ near the south pole of Earth is greater than that of the north pole by approximately eight times, as mentioned in preceding sections. Moreover, it is shown in Fig. 17 that the perigee is moving closer to the north pole (where the argument of perigee is equal to 90 deg for a polar orbit). As the orbital

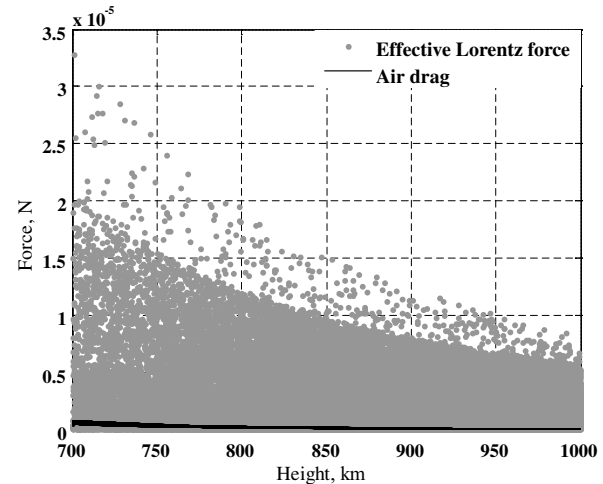


Fig. 14 Details of deorbit forces above 700 km.

altitude continues to decrease the effect of the atmospheric drag starts to exceed the electrodynamic force, leading to the decrease of the orbit eccentricity. The influence of the magnetic field of Earth is less significant in orbits with small inclination angles (see Fig. 15) where the orbit maintains a circular shape all the time if the inclination angle is zero. This variation of eccentricity cannot be noticed if one adopts

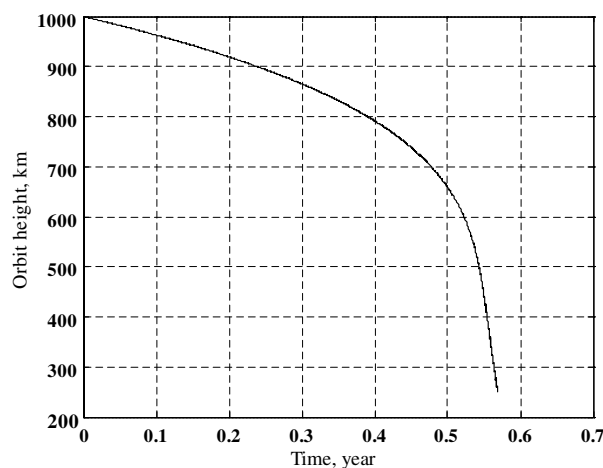


Fig. 15 Deorbit time history of nanosatellites with orbital inclination angle of 0 deg.

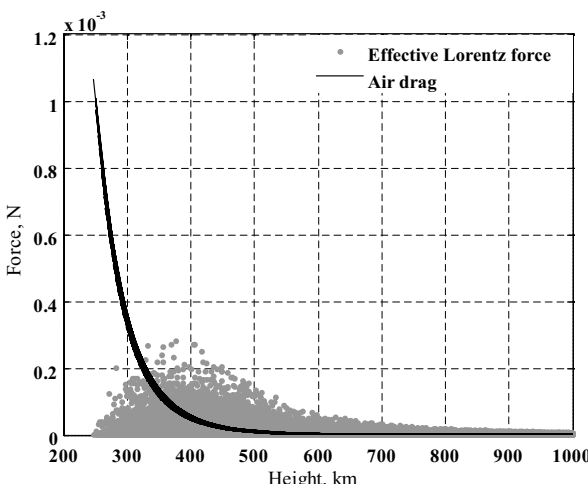


Fig. 13 Variation of deorbit forces acting on EDT in a polar orbit over orbital altitude.

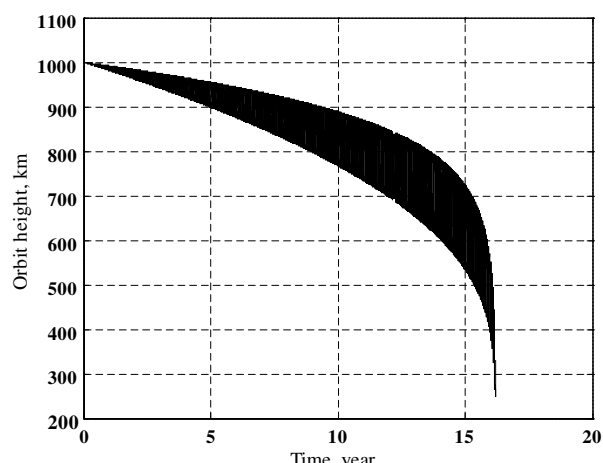


Fig. 16 Deorbit time history of nanosatellites with orbital inclination angle of 90 deg.

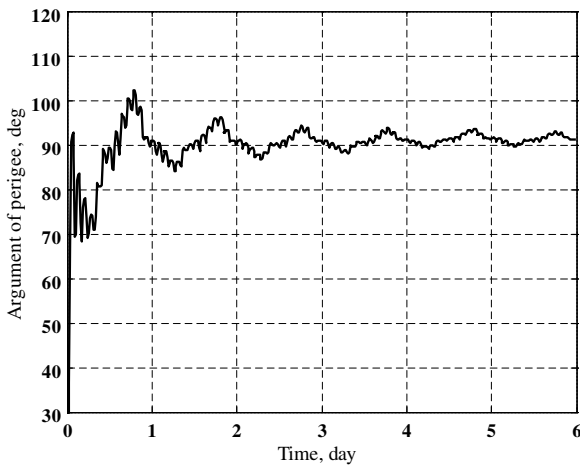


Fig. 17 Variation of argument of perigee for a polar orbit (orbit altitude: 1000 km).

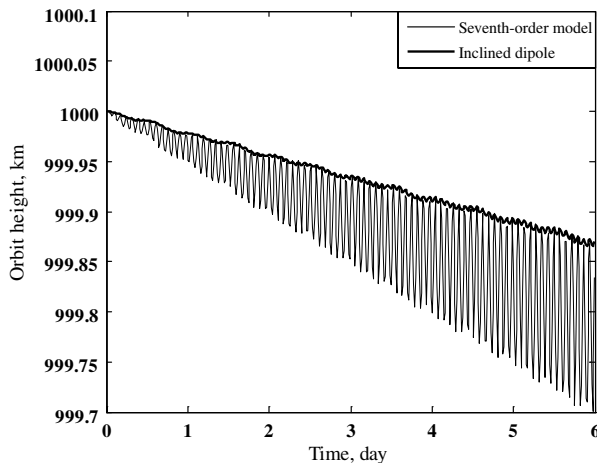


Fig. 18 Deorbit rate using different magnetic-field models for a polar orbit.

the inclined-dipole model of magnetic field that is the first-order approximation of the IGRF2000 model, leading to a less accurate prediction of EDT orbital motion. Detailed results of EDT deorbit in a polar orbit (first 6 days seen in Fig. 18) shows that the large eccentricity of orbit is beneficial to the deorbit process of near-polar orbits using EDT-propulsion technology because a lower perigee leads to a larger atmospheric drag that dissipates the orbital energy of the satellite faster. This is especially important for the polar orbit where the motional electric field is minimal.

V. Conclusions

This paper investigated the dynamics of deorbiting a nanosatellite by an electrodynamic tether. The orbital environmental perturbations including electrodynamic effect are studied in the framework of orbital dynamics of tethered nanosatellite systems in detail. The study reveals that the commonly used inclined-dipole model of Earth's magnetic field is oversimplified for calculating the electrodynamic force exerted on the EDT and will lead to improper orbital-dynamic responses of the system in near-polar orbits. For instance, the orbit of an electrodynamic tether in polar orbits will become elliptical in the deorbit process due to the local strength of Earth's magnetic field, which is much greater near the south pole than the north pole. The orbital-eccentricity variation reaches the maximum in the polar orbit and the minimum in the equatorial orbit. This is specifically beneficial in deorbiting a satellite in polar orbits because the denser atmosphere at a lower perigee provides a larger atmospheric drag to dissipate the orbital energy of the satellite faster. The orbit lifetime

will be reduced by orders of magnitudes with the electrodynamic-tether propulsion in all orbits compared with the atmospheric drag only. Furthermore, the analyses show that the induced motional electric field reverses its direction across the electrodynamic tether in the polar orbit or orbits with higher inclination angles causing the current in the tether to reverse its direction, and consequently, the current-induced electrodynamic force to change its direction. However, the power of electrodynamic force remains negative at all times to dissipate the nanosatellite's orbital energy, which indicates that the electrodynamic force is always acting like a drag to lower the altitude of the tethered-nanosatellite system in all orbits in low Earth orbit.

Acknowledgment

This work is supported by the Discovery Grant of Natural Sciences and Engineering Research Council of Canada.

References

- [1] Bombardelli, C., Lorenzini, E. C., and Quadrelli, M. B., "Retargeting Dynamics of a Linear Tethered Interferometer," *Journal of Guidance, Control, and Dynamics*, Vol. 27, No. 6, 2004, pp. 1061–1067. doi:10.2514/1.2933
- [2] Wen, H., Jin, D., and Hu, H., "Advances in Dynamics and Control of Tethered Satellite Systems," *Acta Mechanica Sinica*, Vol. 24, No. 3, 2008, pp. 229–241. doi:10.1007/s10409-008-0178-6
- [3] Kumar, K. D., "Review of Dynamics and Control of Nonelectrodynamic Tethered Satellite Systems," *Journal of Spacecraft and Rockets*, Vol. 43, No. 4, 2006, pp. 705–720. doi:10.2514/1.5479
- [4] Cartmell, M. P., and McKenzie, D. J., "A Review of Space Tether Research," *Progress in Aerospace Sciences*, Vol. 44, No. 1, 2008, pp. 1–21. doi:10.1016/j.paerosci.2007.08.002
- [5] Puig-Suari, J., "Optimal Mass Flexible Tether for Aerobraking Maneuvers," *Journal of Guidance, Control, and Dynamics*, Vol. 20, No. 5, 1997, pp. 1018–1024. doi:10.2514/2.4149
- [6] Carroll, J. A., "Tether Applications in Space Transportation," *Acta Astronautica*, Vol. 13, No. 4, 1986, pp. 165–174. doi:10.1016/0049-5765(86)90061-5
- [7] Pelaez, J., Lorenzini, E. C., Lopez-Rebollal, O., and Ruiz, M., "A New Kind of Dynamic Instability in Electrodynamic Tethers," *Journal of Astronautical Sciences*, Vol. 48, No. 4, 2000, pp. 449–476.
- [8] Pardini, C., Hanada, T., Krisko, P. H., Anselmo, L., and Hirayama, H., "Are De-orbiting Missions Possible Using Electrodynamic Tethers? Task Review from the Space Debris Perspective," *Acta Astronautica*, Vol. 60, No. 10–11, 2007, pp. 916–929. doi:10.1016/j.actaastro.2006.11.001
- [9] Levin, E., Pearson, J., and Carroll, J., "Wholesale Debris Removal From LEO," *Acta Astronautica*, Vol. 73, 2012, pp. 100–108. doi:10.1016/j.actaastro.2011.11.014
- [10] Jakhu, R. S., "Iridium-Cosmos Collision and Its Implications for Space Operations," in *ESPI Yearbook on Space Policy 2008/2009: Setting New Trends*, Springer-Verlag, New York, 2010, pp. 254–275.
- [11] Steering Committee for NASA Technology Roadmaps, Aeronautics and Space Engineering Board, Division on Engineering and Physical Science, National Research Council of the National Academies, NASA Space Technology Roadmaps and Priorities: Restoring NASA's Technological Edge and Paving the Way for a New Era in Space, National Academies Press, Washington, DC, 2012, pp. E16–E17.
- [12] Kawamoto, S., Makida, T., Sasaki, F., Okawa, Y., and Nishida, S. I., "Precise Numerical Simulations of Electrodynamic Tethers for an Active Debris Removal System," *Acta Astronautica*, Vol. 59, No. 1–5, 2006, pp. 139–148. doi:10.1016/j.actaastro.2006.02.035
- [13] Nishida, S. I., Kawamoto, S., Okawa, Y., Terui, F., and Kitamura, S., "Space Debris Removal System Using a Small Satellite," *Acta Astronautica*, Vol. 65, No. 1–2, 2009, pp. 95–102. doi:10.1016/j.actaastro.2009.01.041
- [14] Jablonski, A. M., and Scott, R., "Deorbiting of Microsatellites in Low Earth Orbit (LEO)—An Introduction," *Canadian Aeronautics and Space Journal*, Vol. 55, No. 2, 2009, pp. 55–67.

- [15] Grossi, M., "Future of Tethers in Space," *Proceedings of 4th International Conference on Tethers in Space, Science and Technology*, Science and Technology Corporation, Hampton, VA, 1995, pp. 11–23.
- [16] Uphoff, C., Forward, R. L., and Hoyt, R. P., "The 'Terminator Tether': An Efficient Mechanism for End-of-Life Deorbit of Constellation Spacecraft," edited by VanDerHa, J. C., Vol. 1, *Mission Design & Implementation of Satellite Constellations*, Kluwer Academic Publishers, Toulouse, France, 1998, pp. 347–365.
- [17] Iess, L., Bruno, C., Ulivieri, C., Ponzi, U., Parisse, M., Laneve, G., Vannaroni, G., Dobrowolny, M., De Venuto, F., Bertotti, B., and Anselmo, L., "Satellite De-orbiting by Means of Electrodynamic Tethers, Part I: General Concepts and Requirements, & Part II: System Configuration and Performance," *Acta Astronautica*, Vol. 50, No. 7, 2002, pp. 399–416.
doi:10.1016/S00094-5765(01)00180-1
- [18] Sanmartin, J. R., Ahedo, E., and Martinez-Sanchez, M., "An Anodeless Tether Generator," *Proceedings of Workshop on Physics of Charged Bodies in Space Plasmas*, edited by Dobrowolny, M., and Sindoni, E., Editrice Compositori, Bologna, Italy, 1992, pp. 201–208.
- [19] Sanmartin, J. R., and Estes, R. D., "The Orbital-Motion-Limited Regime of Cylindrical Langmuir Probes," *Physics of Plasmas*, Vol. 6, No. 1, 1999, pp. 395–405.
doi:10.1063/1.873293
- [20] Sanmartin, J. R., Estes, R. D., Lorenzini, E. C., and Elaskar, S. A., "Efficiency of Electrodynamic Tether Thrusters," *Journal of Spacecraft and Rockets*, Vol. 43, No. 3, 2006, pp. 659–666.
doi:10.2514/1.16174
- [21] Sanmartin, J. R., Lorenzini, E. C., and Martinez-Sanchez, M., "Electrodynamic Tether Applications and Constraints," *Journal of Spacecraft and Rockets*, Vol. 47, No. 3, 2010, pp. 442–456.
doi:10.2514/1.45352
- [22] Bombardelli, C., Herrera-Montojo, J., Iturri-Torrea, A., and Pelaez, J., "Space Debris Removal with Bare Electrodynamic Tethers," *Advances in the Astronautical Sciences*, Vol. 136, Pt. III, 2010, pp. 2523–2533.
- [23] Zhu, Z. H., "Mission Concept of Electrodynamic Tether Flying for Propellantless Propulsion Demonstration and Radio Science Experiment," *The Canadian Society for Mechanical Engineering Bulletin*, Canadian Society for Mechanical Engineering, Kinston, ON, Canada, 2011, pp. 20–27.
- [24] Ahedo, E., and Sanmartin, J. R., "Analysis of Bare-Tether Systems for Deorbiting Low-Earth-Orbit Satellites," *Journal of Spacecraft and Rockets*, Vol. 39, No. 2, 2002, pp. 198–205.
doi:10.2514/2.3820
- [25] Curtis, H. D., *Orbital Mechanics for Engineering Students*, Elsevier, Oxford, 1988, Chap. 4.
- [26] Storch, J. A., "Aerodynamic Disturbances on Spacecraft in Free-Molecular Flow," Aerospace Rept. No. TR-2003(3397)-1, Aerospace Corp., El Segundo, CA, 2002.
- [27] Carroll, J. A., "Guidebook for Analysis of Tether Applications in Tethers," in *Space Handbook*, 3rd ed., edited by Cosmo, M. L., and Lorenzini, E. C., NASA Contract Rept. NASA CR-97-206807, 1997, pp. 152–186.
- [28] Zhu, Z. H., and Zhong, R., "Deorbiting Dynamics of Electrodynamic Tether," *International Journal of Aerospace and Lightweight Structures*, Vol. 1, No. 1, 2011, pp. 47–66.
doi:10.3850/S2010428611000043
- [29] Davis, J., "Mathematical Modeling of Earth's Magnetic Field," TN, Virginia Polytechnic Institute and State Univ., Blacksburg, VA, 2004.
- [30] James, R. W., *Spacecraft Attitude Determination and Control*, D. Reidel Publishing Co., Boston, 1978.
- [31] Khoroshilov, V. S., Pirozhenko, A. V., and Zakrzhevskii, A. E., "Characteristic Properties of Deorbiting of an Electrodynamic Two Cubesat Tether in a Near-Polar Orbit," *Recent Advances in Space Technologies 3rd International Conference*, Istanbul, Turkey, 2007, pp. 176–181.
doi:10.1109/RAST.2007.4283972
- [32] Lanoix, E. L. M., Misra, A. K., Modi, V. J., and Tyc, G., "Effect of Electrodynamic Forces on the Orbital Dynamics of Tethered Satellites," *Journal of Guidance, Control, and Dynamics*, Vol. 28, No. 6, 2005, pp. 1309–1315.
doi:10.2514/1.1759
- [33] Sanmartin, J. R., Martinez-Sanchez, M., and Ahedo, E., "Bare Wire Anodes for Electrodynamic Tethers," *Journal of Propulsion and Power*, Vol. 9, No. 3, 1993, pp. 353–360.
doi:10.2514/3.23629
- [34] Bilitza, D., and Reinisch, B. W., "International Reference Ionosphere 2007: Improvements and New Parameters," *Advances in Space Research*, Vol. 42, No 4, 2008, pp. 599–609.
doi:10.1016/j.asr.2007.07.048
- [35] Wamoeck, T. W., and Cochran, J. E., "Orbital Lifetime of Tethered Satellites," *Journal of the Astronautical Sciences*, Vol. 41, No. 2, 1993, pp. 165–188.
doi:10.2514/1.45352

D. Spencer
Associate Editor